Electronic Supplementary Material (ESI) for Inorganic Chemistry Frontiers.

Supporting Information

Design of Atomically Precise Au_2Pd_6 Nanoclusters for Boosting Electrocatalytic Hydrogen Evolution on MoS_2

Yuanxin Du,[a⊥] *Ji Xiang,*[a⊥] *Kun Ni,*[b] *Yapei Yun,*[a] *Guodong Sun,*[a] *Xiaoyou Yuan,*[a] *Hongting Sheng,*[a] *Yanwu Zhu,*[b] *and Manzhou Zhu*[a]*

[a] Department of Chemistry and Center for Atomic Engineering of Advanced Materials, AnHui Province Key Laboratory of Chemistry for Inorganic/Organic Hybrid Functionalized Materials, Anhui University, Hefei, Anhui 230601, China. E-mail: zmz@ahu.edu.cn

[b] Key Laboratory of Materials for Energy Conversion, Chinese Academy of Sciences, Department of Materials Science and Engineering, Hefei National Laboratory for Physical Sciences at the Microscale, University of Science and Technology of China, 96 Jin Zhai Rd, Hefei, Anhui Province, 230026, China.

[⊥]*Y. Du and J. Xiang contributed equally.*

Table of Contents:

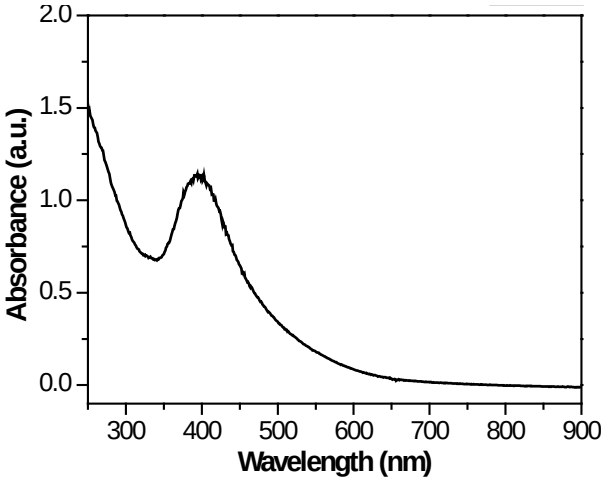

Fig. S1. Optical absorption spectrum of Au_2Pd_6 NC.

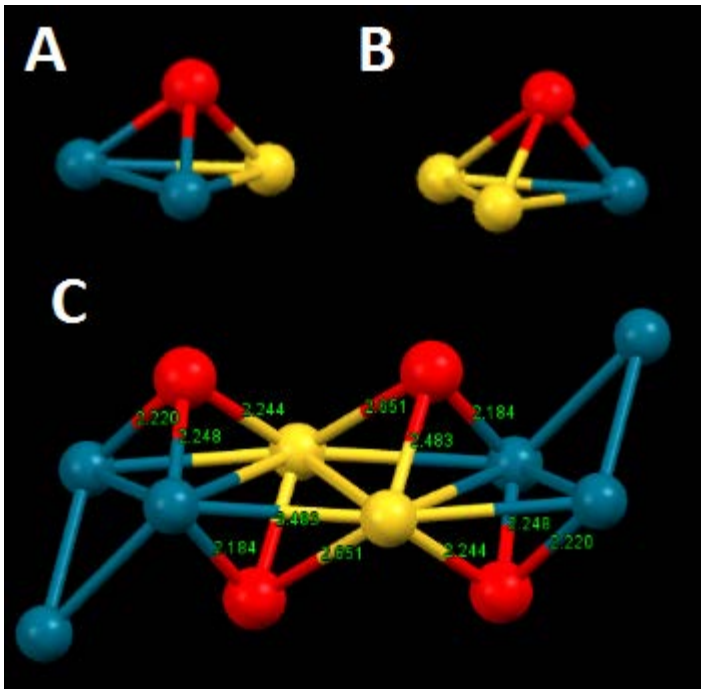

Fig. S2. (A) The one way of one S atom linked to two Pd atoms and one Au atom, (B) the another way of one S atom linked to two Au atoms and one Pd atom, (C) The distance of Au-S, and Pd-S in the Au_2Pd_6 NC. (Color labels: yellow = Au, blue = Pd,

red = S)

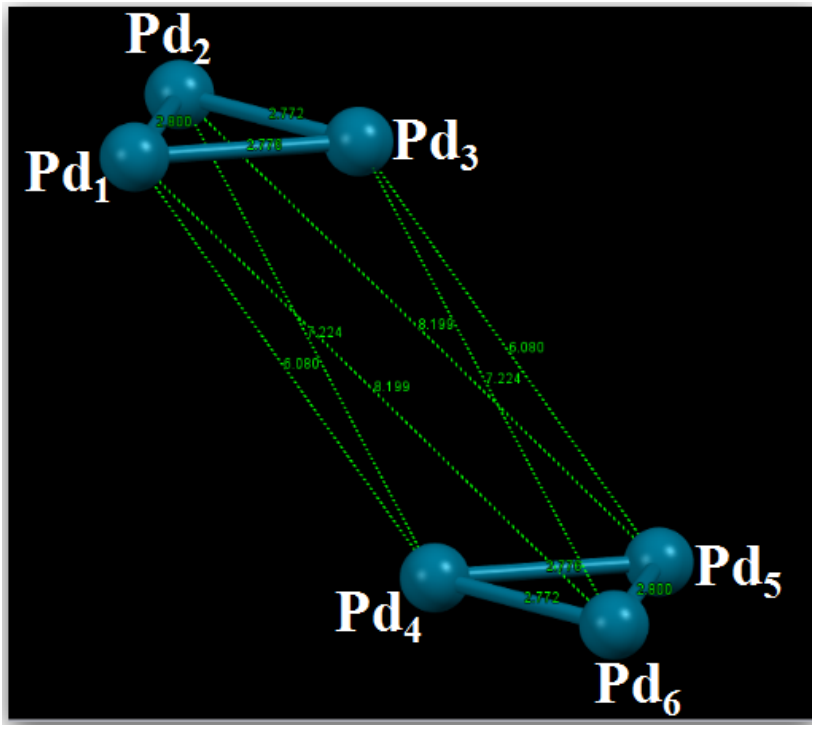

Fig. S3. The distances between Pd atoms in the two triangular Pd_3 units of Au_2Pd_6 NC. From Fig. S3, the Pd-Pd distances in the Pd_3 units were 2.772 Å, 2.776 Å, 2.800 Å. The distances between Pd_3-Pd_6 and Pd_2-Pd_4 were 7.224 Å, the distances between Pd_1-Pd_4 and Pd_3-Pd_5 were 6.080 Å, and the distances between Pd_2-Pd_5 and Pd_1-Pd_6 were 8.199 Å. The quadrangles of $Pd_2Pd_3Pd_6Pd_4$, $Pd_1Pd_3Pd_5Pd_4$, and $Pd_2Pd_1Pd_6Pd_5$ were parallelogram, which means that the two triangular Pd_3 units were paralleled.

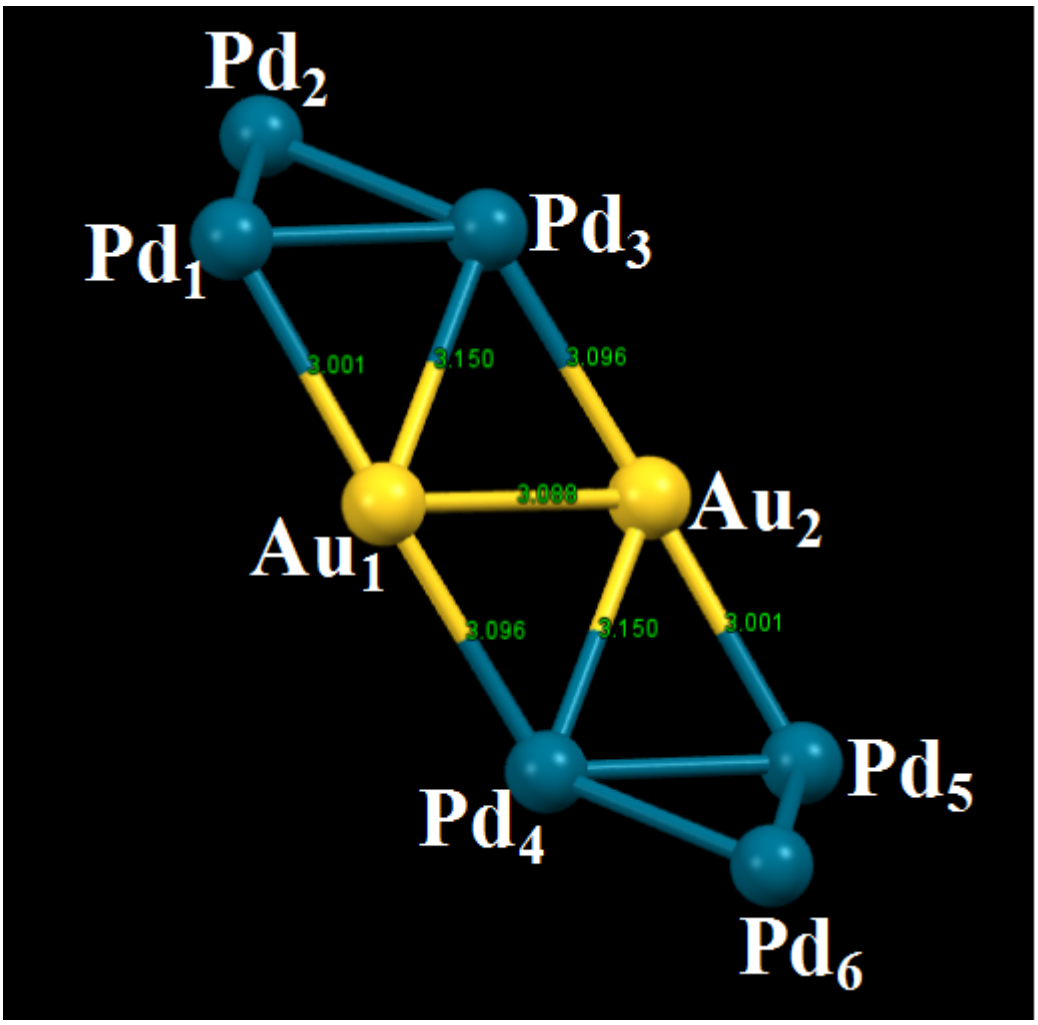

Fig. S4. The distances between the Au and Pd atoms in the Au_2Pd_6 metal core of Au_2Pd_6 NC. In the Au_2Pd_6 core, the distance between Au_1-Au_2 was 3.088 Å, which is greatly larger than the bulk Au-Au distance (2.88 Å). The Au-Pd distances in the Au_2Pd_6 core were 3.001 Å, 3.096 Å, 3.150 Å, respectively.

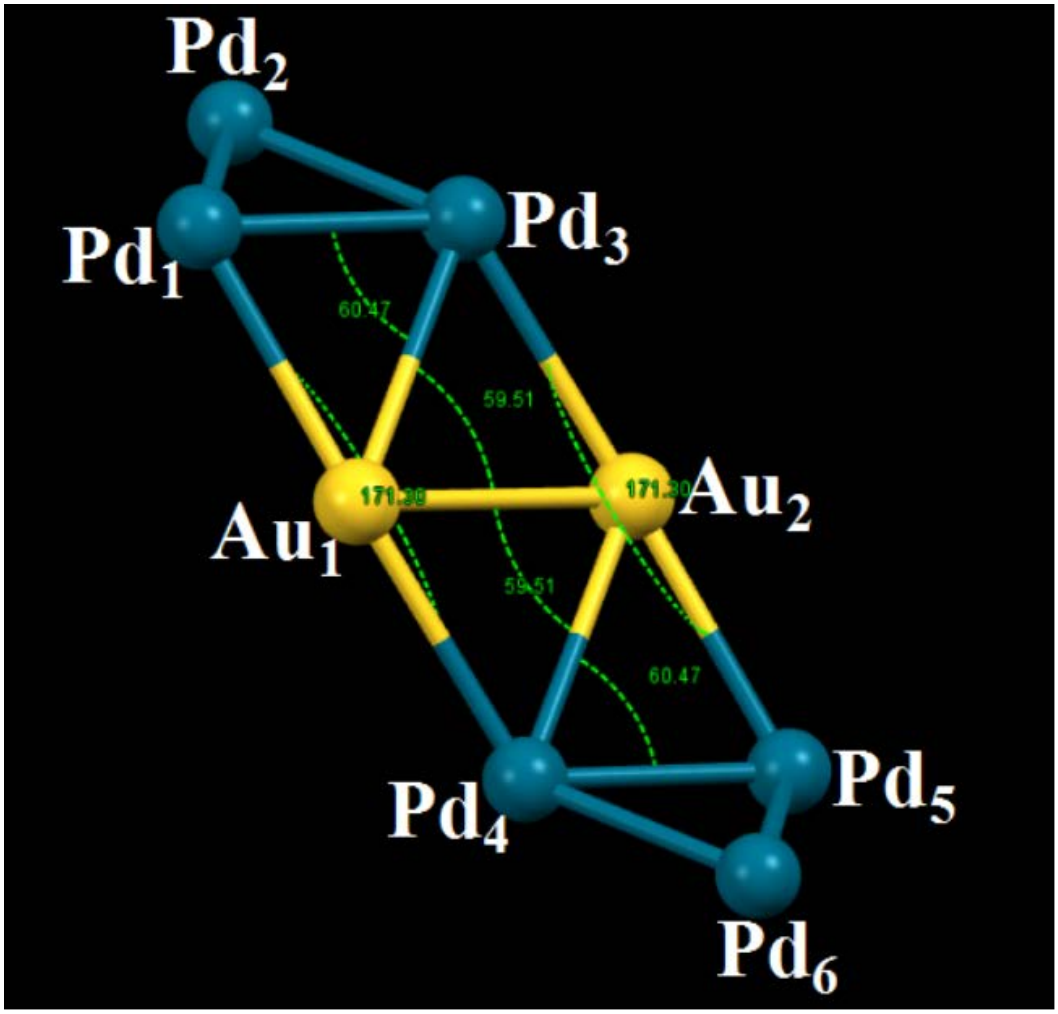

Fig. S5. The angles of Au and Pd atoms in the Au_2Pd_6 metal core of Au_2Pd_6 NC. The angles of Pd_1-Au_1-Pd_4 and Pd_3-Au_2-Pd_5 were 171.30 ˚, the angles of Pd_1-Pd_3-Au_1 and Au_2-Pd_4-Pd_5 were 60.47 °, and the angles of Pd_3-Au_1-Au_2 and Au_1-Au_2-Pd_4 were 59.51°, which means that the quadrangle of $Pd_1Pd_3Au_1Au_2Pd_4Pd_5$ was twisty.

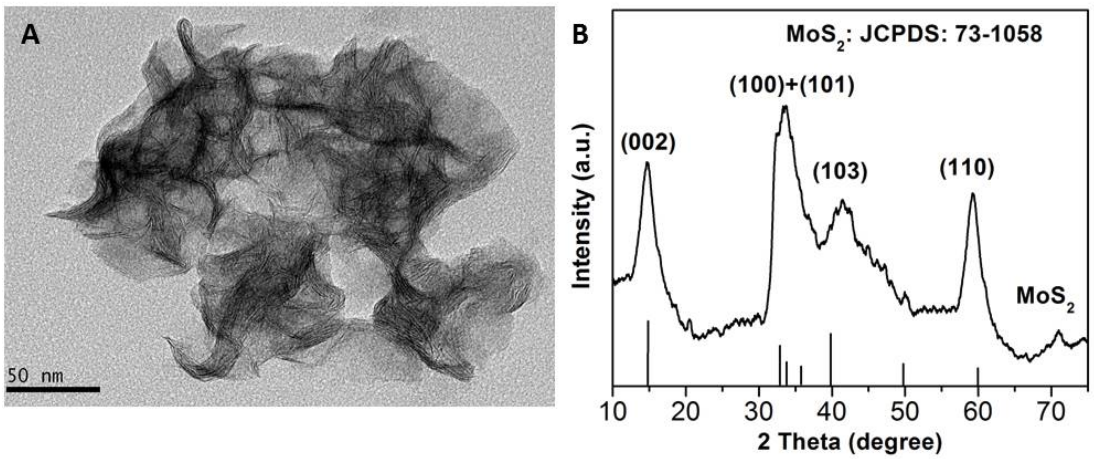

Fig. S6. (A) TEM image and (B) XRD pattern of MoS_2.

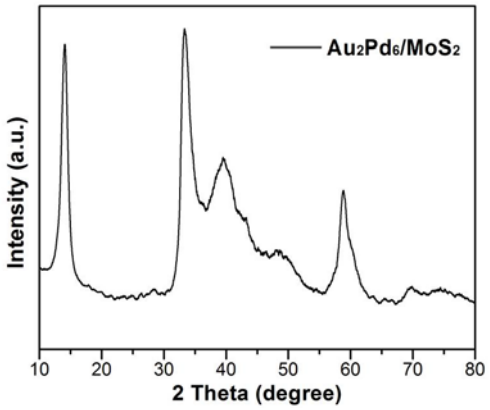

Fig. S7. XRD pattern of Au_2Pd_6/MoS_2.

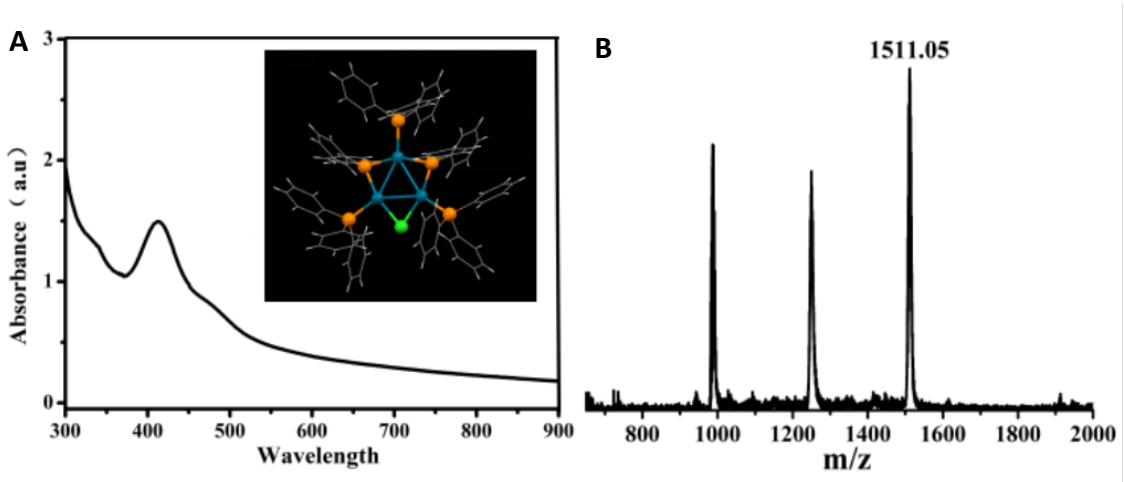

Fig. S8. (A) UV-vis and (B) MALDI-MS spectra of Pd_3 NC. Inset of (A): crystal structure of Pd_3 NC (blue = Pd, deep yellow = P, reseda = Cl). Fig. S8A shows the UV−vis spectrum of Pd_3 NC, in which the peaks at 340, 418, and 485 nm are fingerprints of Pd_3 NC. The X-ray structure of Pd_3 NC (Fig. S8A, inset) comprises a

triangular Pd_3 unit protected by three $–PPh_3$, three $–PPh_2$, and one Cl atom. Fig. S8B shows the matrix-assisted laser desorption ionization mass spectrometry (MALDI-MS) of Pd_3 NC with the molecular ion peak at ~1511.8 Da (theoretical M_w = 1511.05).

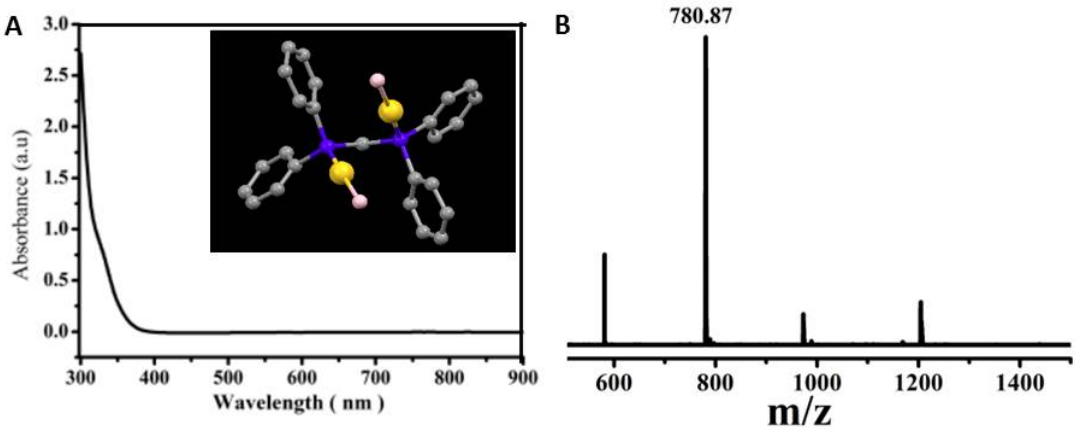

Fig. S9. (A) UV-vis and (B) MALDI-MS spectra of Au_2 complex. Inset of (A): simulated diagram of Au_2 complex crystal structure (yellow = Au, purple = P, pink = Cl). The UV−vis spectrum of Au_2 showed one peak at 330 nm (Fig. S9A). Fig. S9B showed the matrix-assisted laser desorption ionization mass spectrometry (MALDI-MS) of Au_2 with the molecular ion peak at ~780.87 (theretical $[M-2Cl+2H]_w$ =780.155).

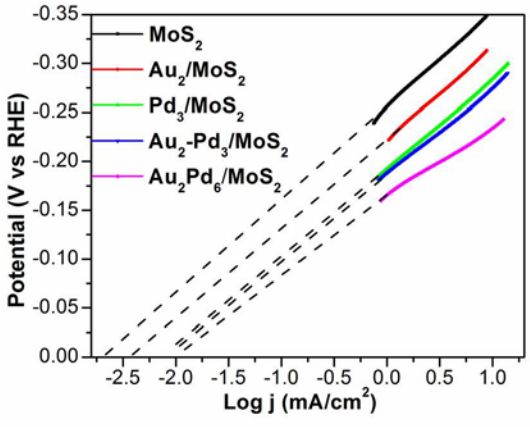

Fig. S10. Exchange current density of various samples calculated using extrapolation methods.

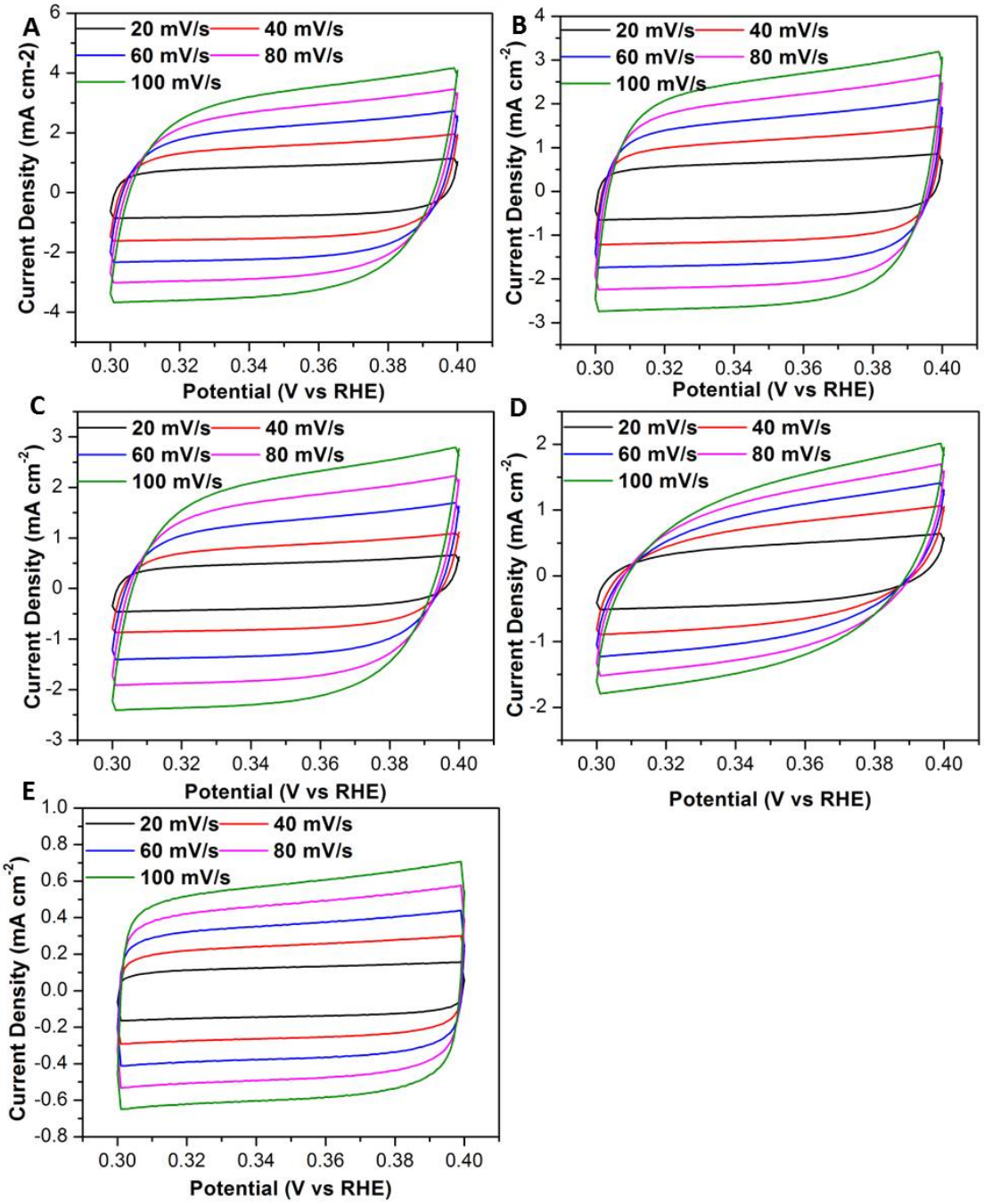

Fig. S11. Cyclic voltammograms (0.3-0.4 V) recorded in 0.5 M H_2SO_4 for (A) Au_2Pd_6/MoS_2, (B) Au_2-Pd_3/MoS_2, (C) Pd_3/MoS_2, (D) Au_2/MoS_2 and (E) MoS_2.

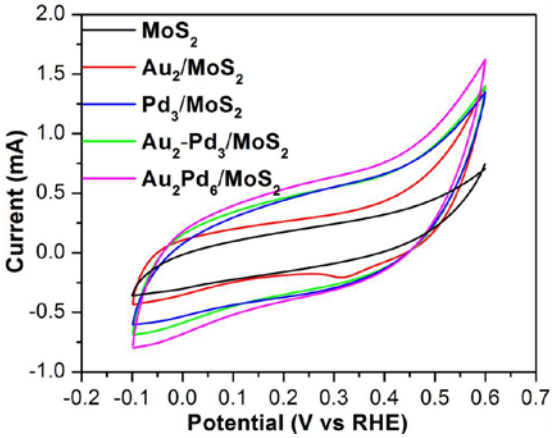

Fig. S12. Cyclic voltammograms (−0.1−0.6 V) recorded in pH = 7 phosphate buffer, scan rate: 50 mV/S.

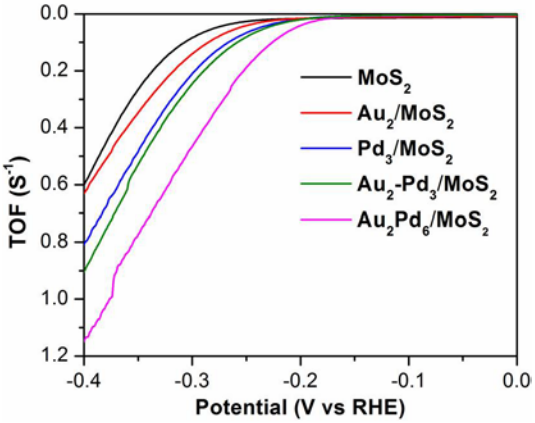

Fig. S13. Calculated turnover frequencies for MoS_2 and various NCs modified MoS_2.

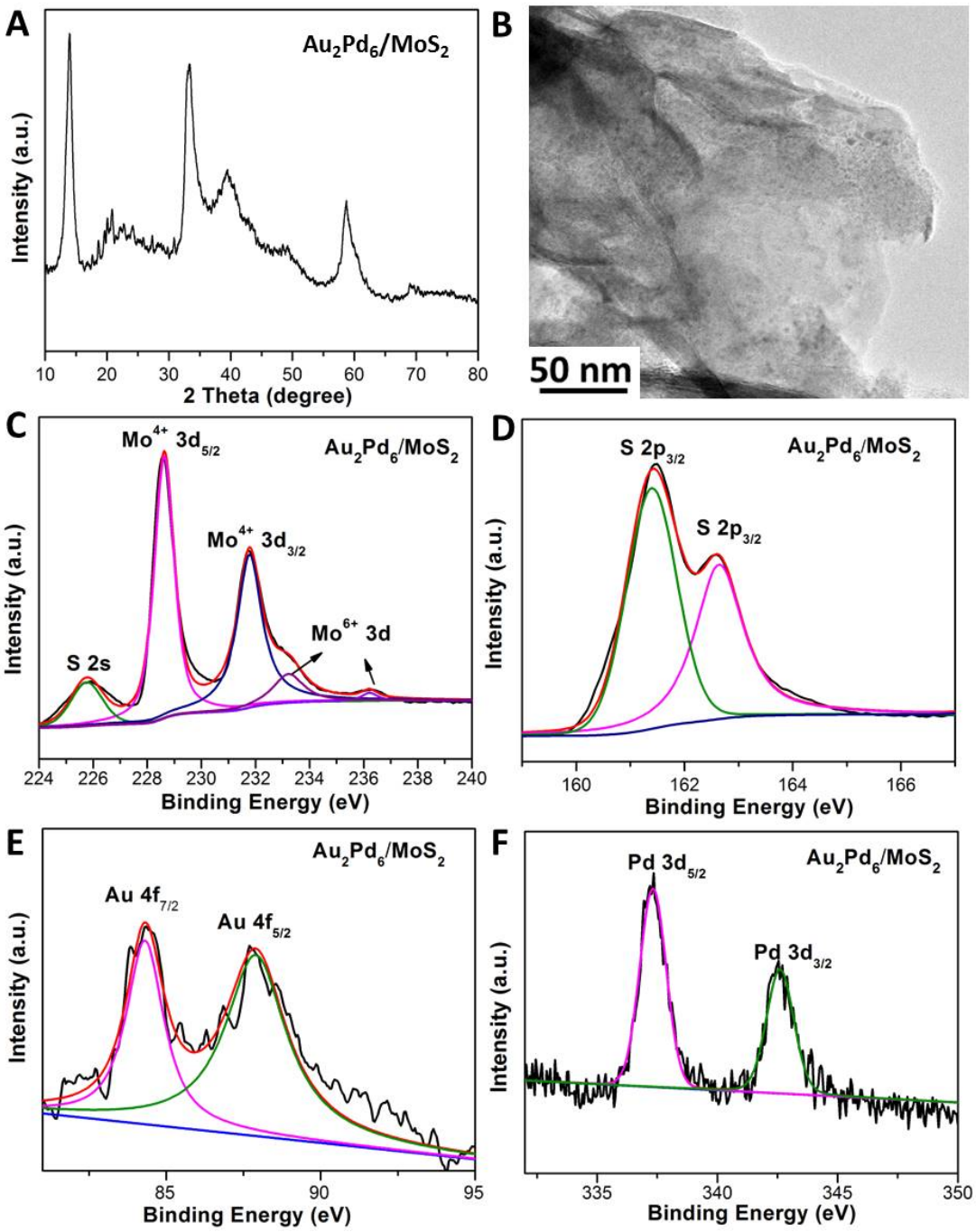

Fig. S14. (A) XRD pattern, (B) TEM image, (C) Mo 3d, (D) S 2p, (E) Au 4f, and (F) Pd 3d XPS spectra of Au_2Pd_6/Mo_{S2} after long-time durability test.

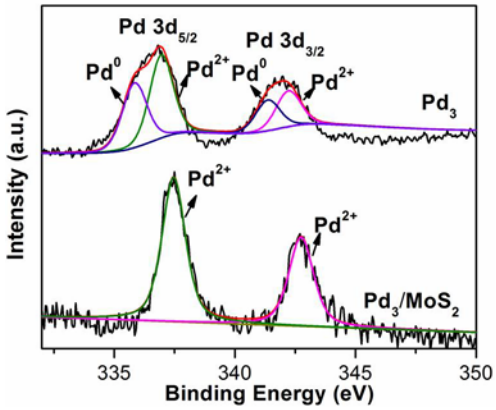

Fig. S15. Pd 3d XPS spectra of Pd_3 and Pd_3/MoS_2.

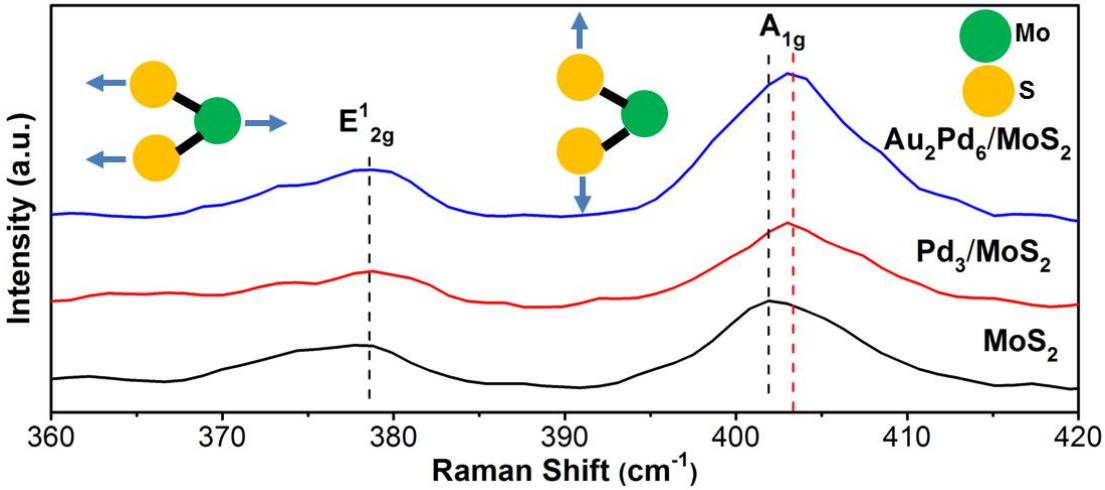

Fig. S16. Raman spectra of MoS_2, Pd_3/MoS_2 and Au_2Pd_6/MoS_2, the inset shows the schematic illustrations of the oscillating modes of $E^1_{2g}$and A_{1g}, respectively. Atom color code: green, Mo; yellow, S.

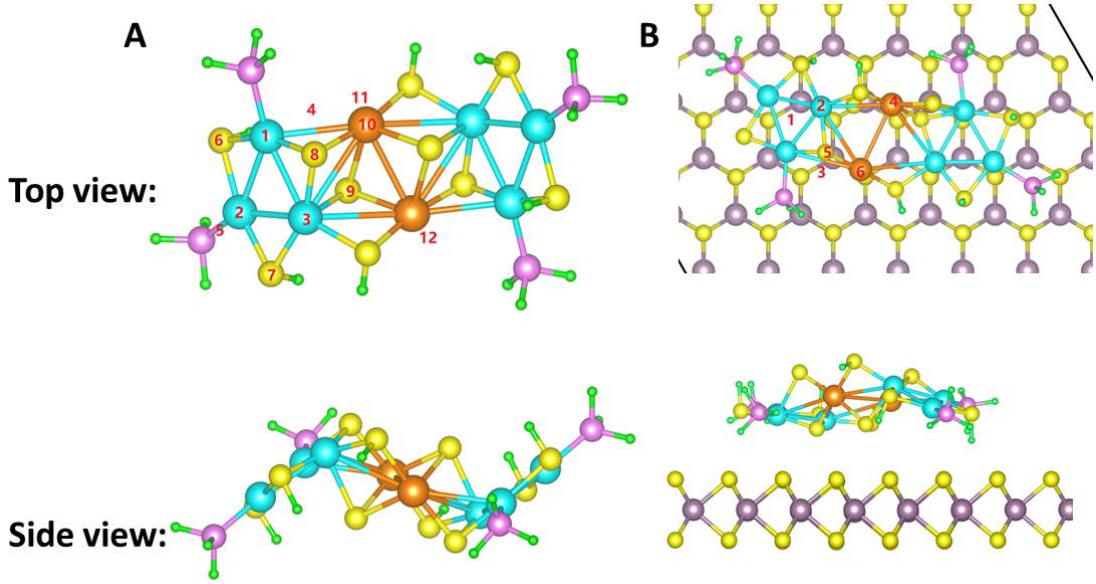

Fig. S17. Different H adsorption sites in (A) Au_2Pd_6 NC system and (B) Au_2Pd_6/MoS_2 system. Yellow ball: S, purple ball: Mo, blue ball: Pd, orange ball: Au, pink ball: P, green ball: H.

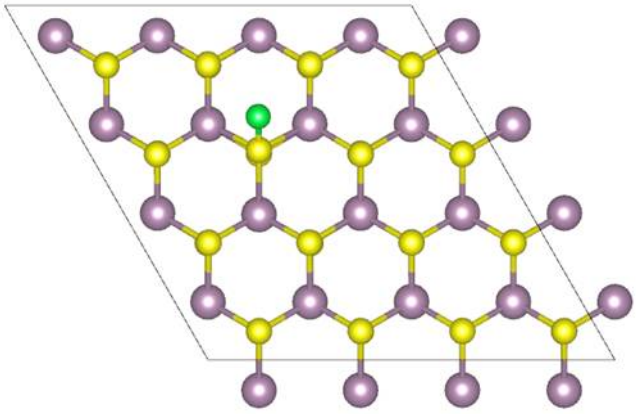

Fig. S18. The optimal H adsorption position in defect-free MoS_2, the corresponding ΔG_H^* is 1.83 eV. Yellow ball: S, purple ball: Mo, green ball: the adsorption H.

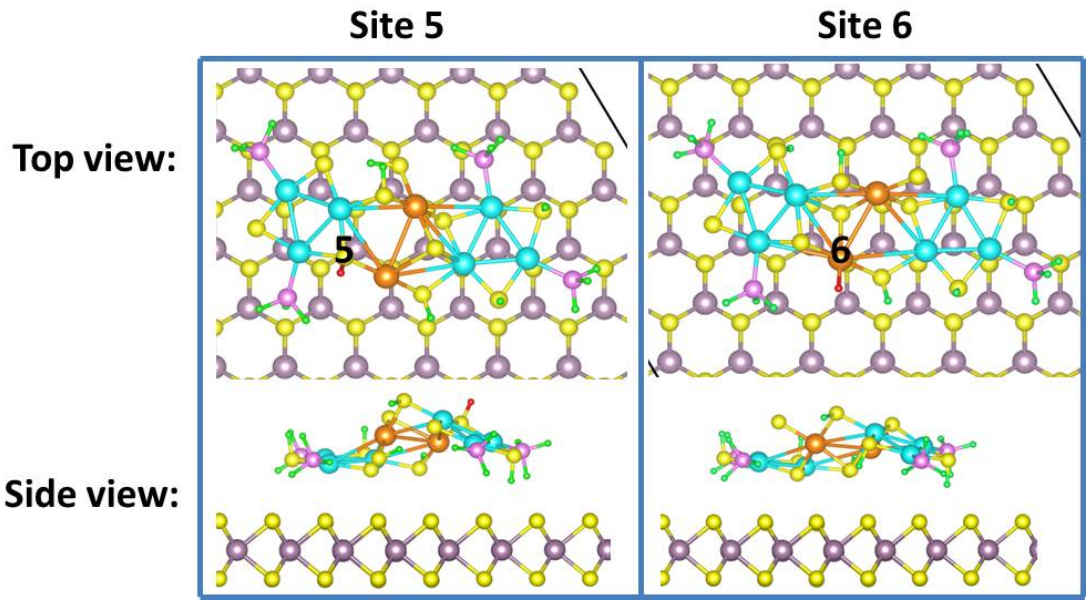

Fig. S19. The specific position of the other two sites with the appropriate ΔG_H^* in Au_2Pd_6/MoS_2 system. Yellow ball: S, purple ball: Mo, blue ball: Pd, orange ball: Au, pink ball: P, green ball: H, red ball: the adsorption H.

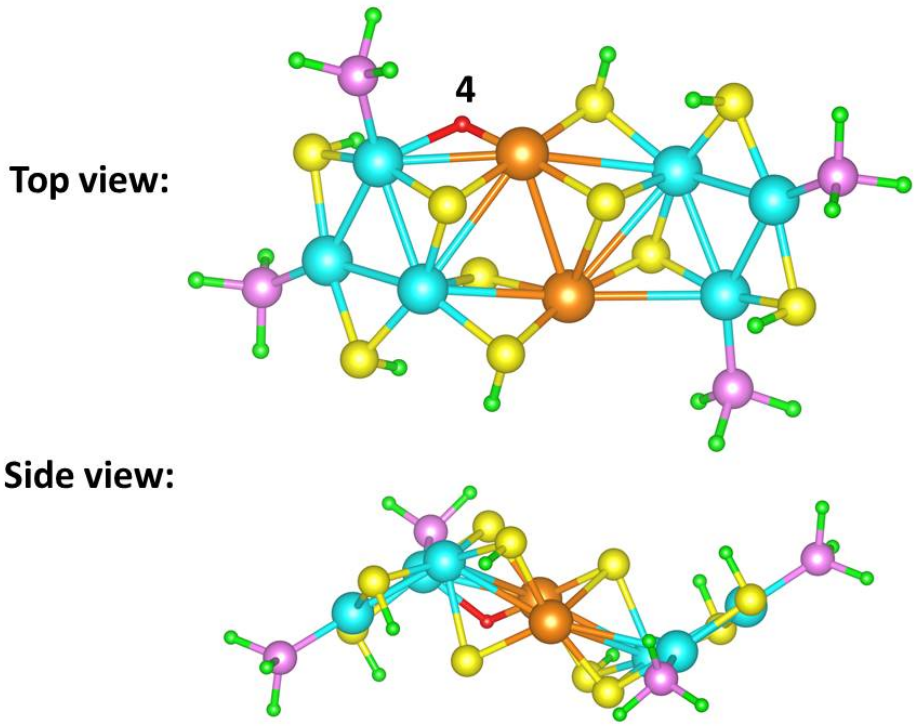

Fig. S20. H adsorption configuration (site 4) in the Au_2Pd_6 NC (from different orientations) with best ΔG_H^* value.Yellow ball: S, blue ball: Pd, orange ball: Au, pink ball: P, green ball: H, red ball: the adsorption H.

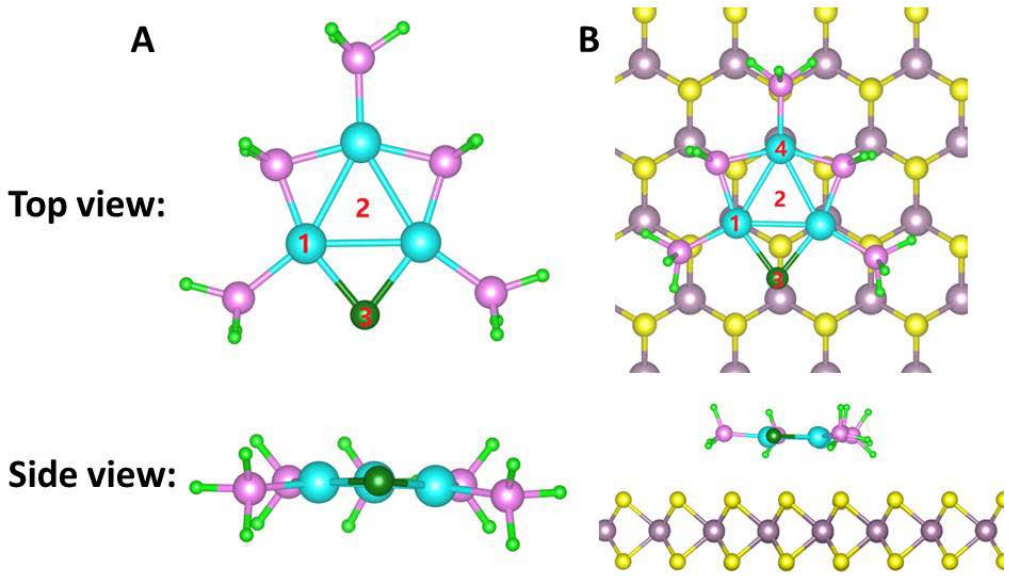

Fig. S21. Different H adsorption sites in (A) Pd_3 NC system and (B) Pd_3/MoS_2 system. Yellow ball: S, purple ball: Mo, blue ball: Pd, pink ball: P, dark green ball: Cl, green ball: H.

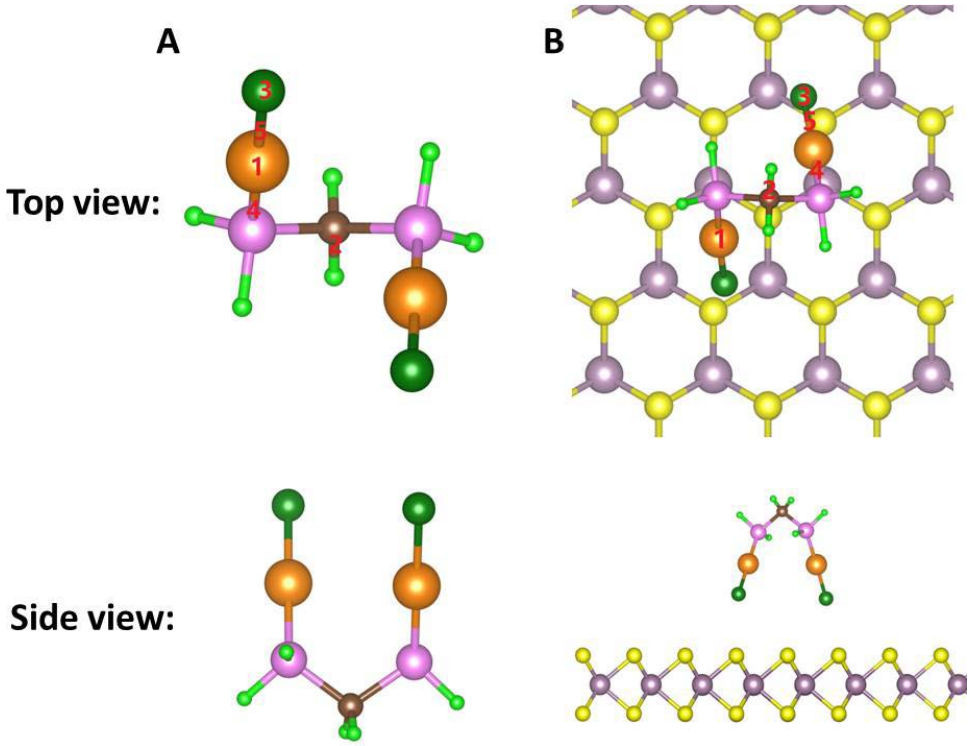

Fig. S22. Different H adsorption sites in (A) Au_2 NC system and (B) Au_2/MoS_2 system. Yellow ball: S, purple ball: Mo, orange ball: Au, pink ball: P, dark green ball: Cl, brown ball: C, green ball: H.

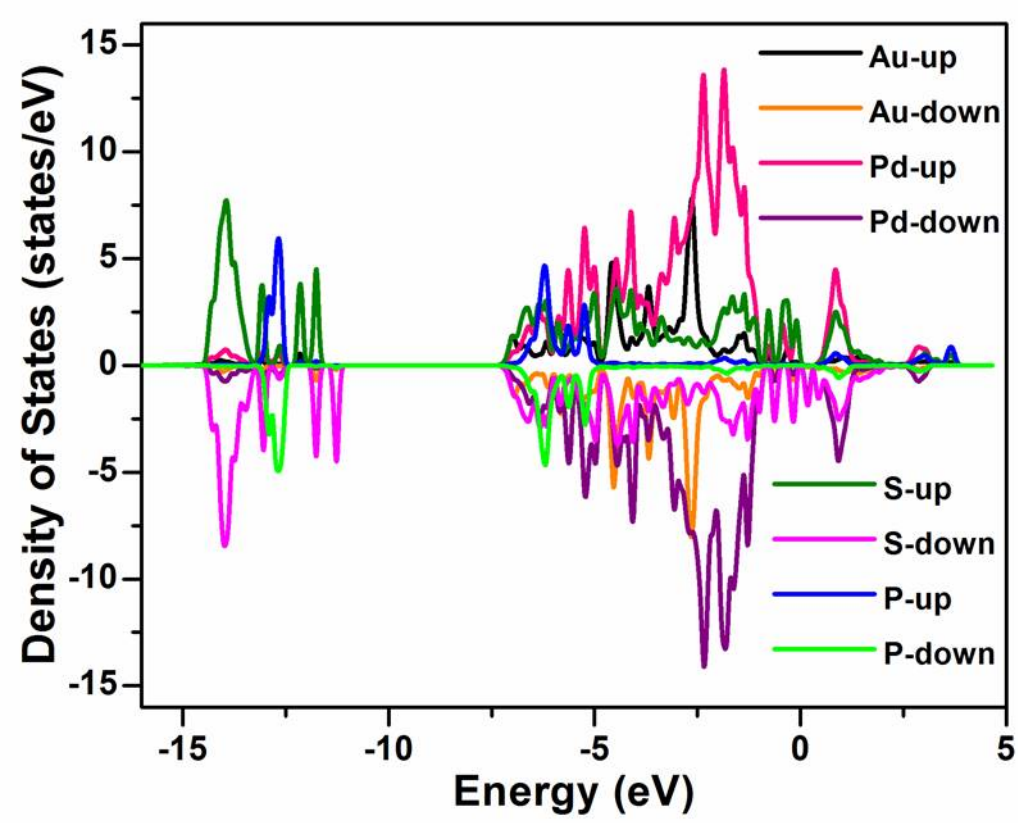

Fig. S23. The density of states of Au, Pd, S and P atoms in the Au_2Pd_6/MoS_2 system.

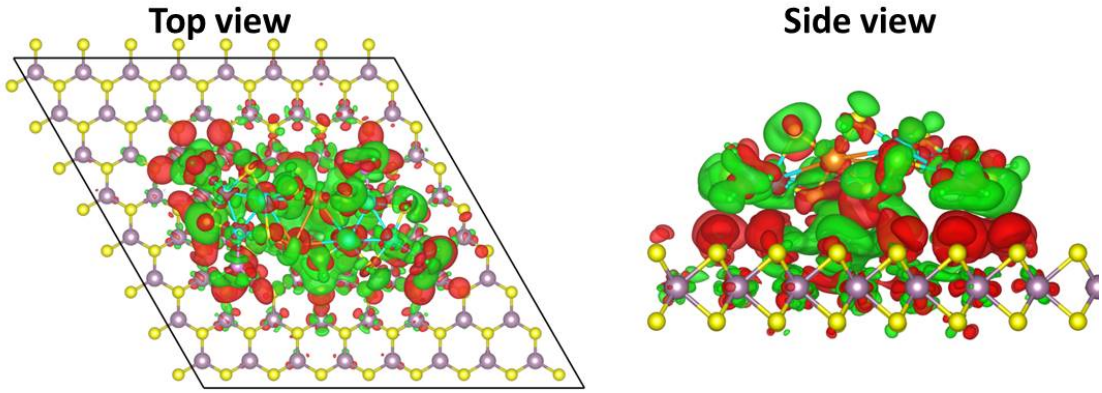

Fig. S24. The charge deformation density of Au_2Pd_6/MoS_2 system. The charge density of Au_2Pd_6 NC is decreased, while the charge density of MoS_2 is increased, it indicates the charge transfer from NC to MoS_2.

Table S1. Electrochemical Parameters of bare MoS_2 and various NCs modified MoS_2.

Catalyst	Onset overpotential (mV)	Overpotential at 10 mA/cm^2 (mV)	Current density at 400 mV (mA/cm^2)	Tafel slope (mV/dec)	Exchange current density (μA/cm^2)	Double layer capacitance (mF/cm^2)	Charge transfer resistance (Ω)	Series resistance (Ω)	The number of Active sites (×10^{-3} mol/g)	TOF at 400 mV (s^{-1})
MoS_2	218	355	20.5	97	2.04	5.69	403	14.13	1.673	0.60
Au_2/MoS_2	180	319	30.1	94	3.89	11.65	329	10.42	2.425	0.63
Pd_3/MoS_2	148	283	53.7	88	7.58	22.48	181	6.82	3.373	0.80
Au_2-Pd_3/MoS_2	141	273	61.7	86	8.31	24.71	178	6.45	3.472	0.90
Au_2Pd_6/MoS_2	127	232	91	67	9.88	32.08	163	6.08	4.02	1.15

Table S2. Comparison of HER performance of MoS_2-based catalysts.

Catalyst	electrolyte	Onset overpotential (mV)	Overpotential at 10 mA/cm^2 (mV)	Current density at 400 mV (mA/cm^2)	Tafel slope (mV/dec)	Exchange current density (μA/cm^2)	Double layer capacitance (mF/cm^2)	Charge transfer resistance (Ω)	Reference
MoS_2	0.5 M H_2SO_4	218	355	20.5	97	2.04	5.69	403	This work
Au_2Pd_6/MoS_2	0.5 M H_2SO_4	127	232	91	67	9.88	32.08	163	This work
Au_{25}/ MoS_2	0.5 M H_2SO_4	200	280	59.3	79.3	-	-	-	1
MoS_2/Au 39.5 mol %	0.5 M H_2SO_4	-	350	22.62	56.97	-	-	162	2
MoS_2-Au (dark)	0.5 M H_2SO_4	220	-	28 [a]	86	-	-	-	3
P. MoS_2/Au	0.5 M H_2SO_4	-	279	-	68.8	0.921	1.6	13	4
Se-doped MoS_2	0.5 M H_2SO_4	140	275 [a]	42.7	55	-	-	650	5
Pt-MoS_2	0.1 M H_2SO_4	-	150	27 [a]	96	-	-	-	6
Pt/MoS_2-80	0.5 M H_2SO_4	31	90 [a]	-	52	-	12.8	8	7

Note: [a] The numerical value was calculated from the figure in the reference.

Table S3. The Gibbs free energy of hydrogen adsorption on different sites in Au_2Pd_6 NC system.

The Gibbs free energy of hydrogen adsorption (ΔG_H^*) on different sites in Au_2Pd_6 system	
Site in Figure S17A	ΔG_H^* (eV)
1	-1.32718
2	-1.3483
3	-1.14434
4	-0.03647
5	-2.22077
6	-0.59976
7	-2.56855
8	-0.87684
9	-3.06807
10	-2.21782
11	-1.41258
12	-1.4237

The calculated ΔG_H^* on different sites in Au_2Pd_6 NC system show that the best H adsorption site is site 4 in Fig. S17A and Fig. S20, the ΔG_H^* on this site is -0.04 eV.

Table S4. The Gibbs free energy of hydrogen adsorption on different sites in Au_2Pd_6/MoS_2 system.

The Gibbs free energy of hydrogen adsorption (ΔG_H^*) on different sites in Au_2Pd_6 /MoS_2 system	
Site in Figure S17B	ΔG_H^* (eV)
1	0.149833
2	0.4319
3	0.295432
4	-0.01148
5	0.022313
6	-0.02848

The calculated ΔG_H^* on different sites in Au_2Pd_6/MoS_2 system show that the best H adsorption site is site 4 in Fig. S17B and Fig. 5A, the ΔG_H^* on this site is -0.01 eV. Meanwhile, site 5 and site 6 also have an appropriate ΔG_H^*, which is 0.02 and -0.03 eV, respectively. The site position is detailedly shown in Fig. S19.

Table S5. The Gibbs free energy of hydrogen adsorption on different sites in Pd_3 NC system.

The Gibbs free energy of hydrogen adsorption (ΔG_H^*) on different sites in Pd_3 system	
Site in Figure S21A	ΔG_H^* (eV)
1	1.418051
2	0.72283
3	1.875788

Table S6. The Gibbs free energy of hydrogen adsorption on different sites in Pd_3/MoS_2 NC system.

The Gibbs free energy of hydrogen adsorption (ΔG_H^*) on different sites in Pd_3 /MoS_2 system	
Site in Figure S21B	ΔG_H^* (eV)
1	1.00724
2	0.961975
3	0.391343
4	0.993066

Table S7. The Gibbs free energy of hydrogen adsorption on different sites in Au_2 NC system.

The Gibbs free energy of hydrogen adsorption (ΔG_H^*) on different sites in Au_2 system	
Site in Figure S22A	ΔG_H^* (eV)
1	1.733362
2	1.560567
3	2.279025
4	1.709955
5	1.705191

Table S8. The Gibbs free energy of hydrogen adsorption on different sites in Au_2/MoS_2 system.

The Gibbs free energy of hydrogen adsorption (ΔG_H^*) on different sites in Au_2 /MoS_2 system	
Site in Figure S22B	ΔG_H^* (eV)
1	1.727127
2	1.55778
3	2.241595
4	1.721984
5	1.686808

References

[1] S. Zhao, R. Jin, Y. Song, H. Zhang, S. D. House, J. C. Yang, R. Jin, *small* **2017**, *13*, 10.1002/smll.201701519.

[2] J. Kim, S. Byun, A. J. Smith, J. Yu, J. Huang, *J. Phys. Chem. Lett.* **2013**, *4*, 1227 −1232.

[3] Y. Shi, J. Wang, C. Wang, T.-T. Zhai, W.-J. Bao, J.-J. Xu, X.-H. Xia, H.-Y. Chen, *J. Am. Chem. Soc.* **2015**, *137*, 7365 −7370.

[4] S. T. Finn, J. E. Macdonald, *ACS Appl. Mater. Interfaces* **2016**, *8*, 25185−25192.

[5] X. Ren, Q. Ma, H. Fan, L. Pang, Y. Zhang, Y. Yao, X. Ren, S. (Frank) Liu, *Chem. Commun.* **2015**, *51*, 15997−16000.

[6] J. Deng, H. Li, J. Xiao, Y. Tu, D. Deng, H. Yang, H. Tian, J. Li, P. Ren, X. Bao, *Energy Environ. Sci.* **2015**, *8*, 1594—1601.

[7] W. Ren, H. Zhang, C. Cheng, *Electrochimica Acta*, **2017**, *241*, 316–322.